Global mode decomposition of supersonic jet noise

By J. W. Nichols, S. K. Lele AND P. Moin

1. Motivation and objectives

The motivation for this research stems from the need to develop noise reduction strategies for aircraft engine exhausts. Because noise production is most significant for high exhaust-to-freestream velocity ratios, exhaust noise is a particular problem at takeoff. Unfortunately, this occurs when the aircraft is in closest proximity to human beings. In commercial aircraft, high bypass-ratio engines lower the velocity ratio by creating a co-annular lower-velocity jet surrounding the main jet core. The large frontal area of high bypass ratio engines makes them impractical for use on supersonic aircraft and other strategies are required to achieve exhaust noise reduction.

Although supersonic jets associated with engine exhaust are typically turbulent, instability wave theory has been somewhat successful at explaining their mechanisms of noise generation (Crighton 1978). The instability wave theory of sound generation hinges upon the existence of coherent large-scale structures, which are known to persist well within the turbulent regime for a variety of free shear flows (Brown & Roshko 1974). The supersonic convection of these orderly structures gives rise to Mach wave radiation, which forms the majority of the supersonic jet noise owing to turbulent mixing (Tam 1995). The other principle components of supersonic jet noise, namely the screech tone and the broadband shock-associated noise, are absent in the perfectly expanded jets we consider in this paper.

Linear stability analyses of compressible round jets based on parallel (see Michalke 1984) and weakly non-parallel (Tam & Burton 1984) flow have yielded a wealth of information regarding the Kelvin–Helmholtz instability responsible for the creation of large-scale coherent structures. Additionally, Tam & Hu (1989) showed the existence of two other families of subsonic and supersonic instability waves in high-speed jets. In the context of a parallel vortex sheet model of a high speed jet, the subsonic instability waves have subsonic phase velocity in the fluid exterior to the jet and are present no matter the jet Mach number. On the other hand, the supersonic instability waves are only appear in strongly supersonic jets.

Although turbulent jets may support instability waves, they are less parallel than their laminar counterparts. Particularly, the collapse of the potential core of a turbulent jet may produce a strongly non-parallel change in spreading rate in a region that is thought to be key to sound production. Therefore, the applicability of parallel or weakly parallel theory to turbulent jets is less than clear.

More recently, the parabolized stability equations (PSE) have been applied as a better model of instability waves in non-parallel supersonic jets (Malik & Chang 2000), resulting in better agreement with the experimental results of Morrison & McLaughlin (1980). Using the nonlinear PSE coupled with an acoustic analogy, Cheung *et al.* (2007) have shown that this agreement can be extended to jets containing Kelvin–Helmholtz stability waves with subsonic convection velocities. The PSE methodology, however, cannot capture upstream propagating waves, and breaks down in cases associated with strong heating (Cheung & Lele 2009).

Recently, there has been renewed interest in instability wave theory as a basis to explain sound production in subsonic jets. Although the large-scale coherent structures cannot directly radiate sound in subsonic jets, Sandham *et al.* (2006) show that energy can be transferred into the radiative part of the spectrum through nonlinear interaction of two instability waves. Using direct numerical simulation (DNS), Suponitsky & Sandham (2009) studied the response of a nonlinear jet to eigenfunction forcing at two different frequencies, and found that the difference mode interaction is most effective at radiating acoustic energy. Furthermore, Wu & Huerre (2009) showed that the interaction of two helical modes of nearly the same frequency but opposite azimuthal wavenumber generated a slowly breathing mean-field distortion of azimuthal wavenumbers $m = \pm 2$ that efficiently radiates low-frequency sound. These previous investigations have focused on the quadratic interactions between pairs of forced modes. Also, the results of these investigations are sensitive to the amplitude of the forcing.

The objective of the present study is to analyze the mechanisms of sound generation in high-speed jets by global mode decomposition. In this context, a global mode of the system has the form

$$\boldsymbol{q}'(x, r, \theta, t) = \hat{\boldsymbol{q}}(x, r) e^{i(m\theta - \omega t)}, \tag{1.1}$$

where $\hat{\boldsymbol{q}}$ is an eigenfunction of the full system extended in both the axial and radial directions. Global modes naturally capture both the non-parallelism of the base flow and upstream wave propagation. The rise of modern computing power, coupled with the development of powerful Krylov-subspace iterative methods, have recently made the problem of extracting global modes tractable. Once a basis of global modes is extracted, it may be used to study the transient response of the system through superposition. This analysis suggests which combinations of linear modes amplify the most, thus determining which nonlinear interactions are most likely.

2. Flow configuration and governing equations

2.1. *Geometry*

A cross-sectional schematic of noise production from a round, supersonic jet is shown in Fig. 1. The computations in this paper use cylindrical coordinates with x, r, and θ denoting the axial, radial and azimuthal directions, respectively. The base flow, corresponding to a steady laminar jet, is assumed to be axisymmetric† with respect to the centerline of the domain, shown at bottom. The jet enters the computational domain from the left through a round nozzle at $x = 0$ and forms a shear layer as it encounters quiescent fluid within the domain. Depending upon the flow parameters, the shear layer exhibits hydrodynamic instabilities that, in the case of a supersonic jet, may couple directly with the acoustic far field through a mechanism of Mach wave radiation.

2.2. *Governing equations*

The fully compressible Navier–Stokes equations are used as a mathematical model describing the dynamics of the supersonic jet. These equations govern the evolution of the system state $\boldsymbol{q} = [p\ \boldsymbol{u}\ s]^T$ where p, $\boldsymbol{u}$, and s are the fluid pressure, velocity, and entropy,

† This does not preclude swirling, axisymmetric jets, although swirl is not considered for the purposes of this article.

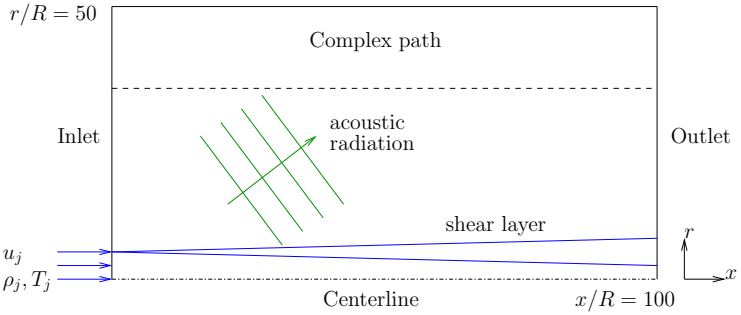

FIGURE 1. A schematic of the flow configuration under consideration. An axisymmetric supersonic jet enters the computational domain from left. For supersonic jets, shear layer instability waves may couple directly to acoustic modes, which radiate to the far field.

respectively. Written in nondimensional form, these equations are:

$$\begin{aligned}
\frac{\partial p}{\partial t} &+ \boldsymbol{u}\cdot\nabla p + \rho c^2 \nabla\cdot\boldsymbol{u} &&= \frac{1}{M^2 Re Pr}\nabla^2 T,\\
\frac{\partial \boldsymbol{u}}{\partial t} &+ \frac{1}{\rho}\nabla p + \boldsymbol{u}\cdot\nabla\boldsymbol{u} &&= \frac{1}{Re}\frac{1}{\rho}\nabla\cdot\boldsymbol{\tau},\\
\frac{\partial s}{\partial t} &+ \boldsymbol{u}\cdot\nabla s &&= \frac{1}{(\gamma-1)M^2 Re Pr}\frac{1}{\rho T}\nabla^2 T.
\end{aligned} \tag{2.1}$$

In the above, the fluid density ρ and temperature T are related to the pressure through the equation of state for an ideal gas: $\gamma M^2 p = \rho T$. Furthermore, the entropy is defined in terms of pressure and temperature as $s = \ln(T)/((\gamma-1)M^2) - \ln(p)/(\gamma M^2)$ so that $s = 0$ when $p = 1$ and $T = 1$. The local speed of sound is defined as $c = \sqrt{\gamma p/\rho}$, and $\boldsymbol{\tau}$ represents the viscous stress tensor.

The equations have been nondimensionalized with respect to the nozzle radius R as well as the jet velocity, density and temperature at the inlet, denoted u_j, ρ_j, and T_j, respectively. This choice of scales is often used in literature describing high speed jet aeroacoustics, and yields a Reynolds number $Re = \rho_j u_j R/\mu$ half that of a Reynolds number based on nozzle diameter, another common choice of characteristic length scale. The Prandtl number is likewise defined as $Pr = c_p\mu/\lambda$, where c_p is the specific heat at constant pressure, μ is the dynamic viscosity, and λ is the thermal conductivity, all of which are assumed to be constant throughout the entire fluid, and, for simplicity, are such that $Pr = 1$. The jet Mach number is defined as $M^2 = u_j^2/(\gamma\mathcal{R}T_j)$, where $\mathcal{R}$ is the specific gas constant and γ is the ratio of specific heats with constant value of 1.4.

The steady base flow should satisfy the nonlinear system (2.1) with temporal and azimuthal derivatives identically zero. For slowly developing jets, approximate solutions are obtained by solving the compressible boundary layer equations together with the Crocco-Busemann relation. The solution is marched from a given inlet condition downstream using the method of Lu & Lele (1996). An iterative scheme is employed to construct a radial velocity profile satisfying the continuity equation at the inlet.

To investigate the behavior of small perturbations about the base flow, we linearize the fully compressible Navier–Stokes equations by decomposing the state variables $\boldsymbol{q} = \bar{\boldsymbol{q}} + \boldsymbol{q}'$ into steady and fluctuating parts, denoted by overbars and primes, respectively. Retaining

only the first-order terms in $\boldsymbol{q}'$ results in the following system of linear equations.

$$\begin{aligned}
&\frac{\partial p'}{\partial t} + \bar{\boldsymbol{u}}\cdot\nabla p' + \bar{\rho}\bar{c}^2\nabla\cdot\boldsymbol{u}' + \gamma\left(\nabla\cdot\bar{\boldsymbol{u}}\right)p' = \frac{\gamma-1}{RePr}\nabla^2\left[\bar{T}(p'+s')\right],\\
&\frac{\partial \boldsymbol{u}'}{\partial t} + \frac{1}{\bar{\rho}}\nabla p' + \bar{\boldsymbol{u}}\cdot\nabla\boldsymbol{u}' + \boldsymbol{u}'\cdot\nabla\bar{\boldsymbol{u}} = \frac{1}{Re}\left\{\frac{1}{\bar{\rho}}\nabla\cdot\boldsymbol{\tau}' - \frac{M^2\nabla\cdot\bar{\boldsymbol{\tau}}}{\bar{\rho}}\left[p'-(\gamma-1)s'\right]\right\},\\
&\frac{\partial s'}{\partial t} + \bar{\boldsymbol{u}}\cdot\nabla s' + \boldsymbol{u}'\cdot\nabla\bar{s} = \frac{1}{RePr}\left\{\nabla^2\left[\bar{T}(p'+s')\right] - \frac{\gamma}{\gamma-1}p'\nabla^2\bar{T}\right\}.
\end{aligned} \tag{2.2}$$

Here, we have also assumed that the supersonic jet is perfectly expanded with a constant base pressure $\bar{p} = 1/(\gamma M^2)$ so that $\bar{\rho}\bar{T} = 1$. For convenience, the primes on fluctuating quantities will be dropped henceforth.

For damped modes, the condition of radiation does not necessarily imply that the solution vanishes as $r \to \infty$. However, the condition of radiation applied along a complex path $r = ae^{i\phi}$, where a is a real-valued variable and ϕ is a small constant positive angle, produces vanishing solutions as $a \to \infty$ that can be resolved numerically (Riedinger *et al.* 2010). For our calculations, we take a hybrid approach where r is real in the range $0 < r < 33.5$ after which it follows the complex ray $r = 33.5 + (a - 33.5)e^{i\pi/10}$ for $33.5 < a < 50$. Dirichlet boundary conditions are then enforced at $a = 50$. Following Ehrenstein & Gallaire (2005), inlet and outlet conditions are matched to the local dispersion relation employing a Gaster-type transformation.

Fourth-order centered finite differences applied on a stretched mesh yield a large sparse matrix. By inverting this matrix about a complex shift, eigenvalues close to the shift become the largest of the new system and can be converged efficiently using the implicitly restarted Arnoldi method (IRAM), which is part of the public domain software package ARPACK (Lehoucq *et al.* 1998). The inversion step is computed by finding the LU decomposition of the shifted sparse matrix using the massively parallel SuperLU package (Li & Demmel 2003). For each shift, the computationally expensive LU decomposition needs to be performed only once, after which the resulting factors are applied repeatedly at each step of the iterative Arnoldi process, thereby improving the overall computational efficiency of the method.

Finally, because centered differences are used to construct the system matrix, the resulting numerical scheme is non-dissipative, except for viscous effects. In some cases, therefore, it may be desirable to add a small amount of scale-selective artificial dissipation to damp spurious modes associated with the smallest wavelengths allowed by the mesh. The numerical filter is introduced by adding terms of the forms $\epsilon\left(\partial^4 q/\partial x^4\right)$ and $\epsilon\left(\partial^4 q/\partial r^4\right)$, which may be discretized with the same stencil width as the original scheme, to the right hand side of (2.2). Here, q represents a state variable and ϵ is a small parameter regulating the filter strength. As discussed in the following section, the filter does not affect the discrete modes of interest if they are well resolved by the mesh.

3. Results

3.1. *Validation and verification*

3.1.1. *Locally parallel stability*

To verify that the numerical method produces correct results, we first compare it to a case studied by Malik & Chang (2000), in which the stability of the supersonic jet is

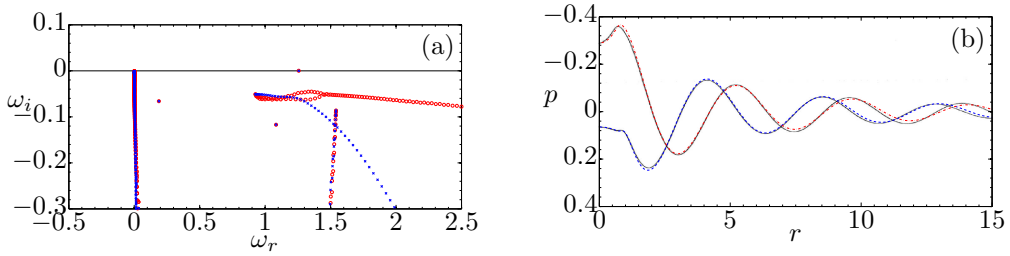

FIGURE 2. (a) Spectra obtained for 1D eigenvalue problem, with (×) and without (○) the filter. (b) Pressure eigenfunction shape of neutral mode: data taken from Malik & Chang (2000) ——, real part – – – , and imaginary part —·— of present calculations.

considered under the assumption of locally parallel flow. For this case, a half-Gaussian inlet profile was selected with initial shear layer thickness $\delta = 0.031$. The flow parameters were $Re = 4350$, $M = 2.5$, and $T_j/T_0 = 0.444$ where T_0 denotes the temperature of the ambient fluid. These flow conditions correspond to a cold, supersonic jet. Because the Reynolds number in this case is slightly higher than that used in the rest of this paper, we expect the solutions of this case to exhibit sharper gradients, especially in the vicinity of the shear layer. In this respect, this case serves as a rigorous test of the numerical method.

For locally parallel flow, solutions to the eigenvalue problem are assumed to take the following form in which an axial wavenumber k is introduced:

$$\boldsymbol{q}'(x, r, \theta, t) = \tilde{\boldsymbol{q}}(r) e^{i(kx + m\theta - \omega t)}. \tag{3.1}$$

In this case, the stability problem reduces to a one-dimensional eigenvalue problem. This is implemented in the developed code by limiting the axial resolution to one grid point and replacing subroutines for axial derivatives with subroutines simply multiplying state variables by ik. This provides a direct test of the code later used to compute fully nonparallel global modes.

Using this method, a spectrum of eigenfrequencies (×) of the system matrix with included numerical filter is displayed in Fig. 2(a) for $k = 1.542 - 0.083i$. In this figure, the real part of ω, plotted along the horizontal axis, corresponds to the temporal frequency of the corresponding eigenfunctions. Likewise, the imaginary part of ω, plotted along the vertical axis, represents the temporal growth rate. Since all of the eigenfrequencies (except one) have negative imaginary parts, all of the modes (except one) are damped at this wavenumber. The remaining neutral mode corresponds to "mode 1" of Malik & Chang (2000). The corresponding mode shape is shown in Fig. 2(b) and agrees closely to the shape found by Malik & Chang (2000).

The effect of removing the numerical filter is also shown in Fig. 2(a). Note that the spectrum is composed of a few discrete modes as well as a "continuous spectrum." The discrete modes arise from the interior of the jet bounded by the shear layer at finite radius, whereas the continuous spectrum, composed of branch cuts, arises from the unbounded nature of the domain exterior to the jet. In particular, without the filter (○), the nearly horizontal branch cut at slightly damped values of ω_i corresponds to acoustic modes of the fluid outside of the jet. Because these modes propagate at constant velocity c, the radial wavenumber is directly proportional to the frequency. The filter therefore has the effect of damping high-frequency modes corresponding to short wavelengths. On the other hand, note that the position of the eigenvalues of the discrete modes are unaffected by the filter, as these modes are well resolved by the chosen mesh.

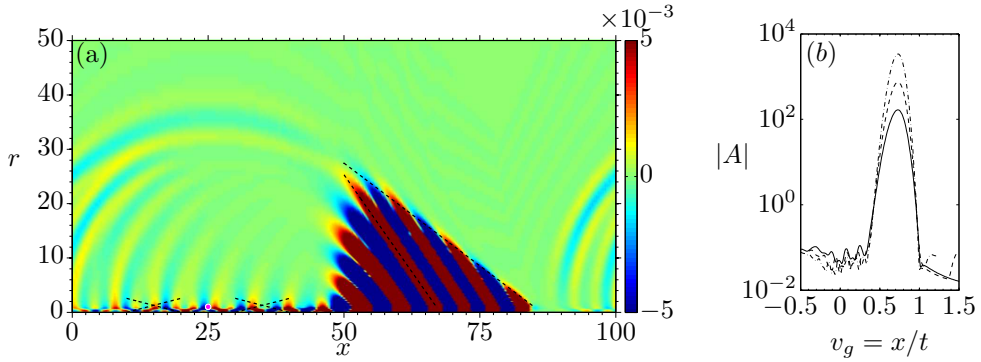

FIGURE 3. (a) Linear response at time $t = 60$ of the artificially parallel supersonic jet to an initial pressure disturbance localized at $(x, r) = (25, 1)$. The acoustic response is contained within a Mach cone indicated by the dashed line farthest to the right. The other dashed lines indicate angles associated with instability waves predicted by the theory of Tam & Hu (1989). (b) Wavepacket amplitude versus group velocity at $t = 40$ ——— , 50 - - - - , and 60 —·— .

3.2. *Linear impulse response of a parallel supersonic jet*

Before considering global modes about a spatially developing base flow, it is informative to consider first the linear impulse response about an artificially parallel supersonic jet. For this section, and for the rest of this paper, we consider a cold supersonic jet with $Re = 3600$, $M = 2.5$, and $T_j/T_0 = 0.444$. At the inlet, we use profile #2 of Michalke (1984) for the axial velocity. An artificially parallel base flow is constructed by imposing the inlet conditions at every axial location. The domain is periodic in the axial direction. Because helical modes are known to have the strongest growth rate (Malik & Chang 2000), we restrict our analysis in this and following sections to perturbations of azimuthal wavenumber $m = 1$.

Fig. 3(a) shows the linear response of the parallel jet to an impulsive pressure perturbation at $(x, r) = (25, 1)$. Owing to antisymmetry of the $m = 1$ mode, this also introduces an equal and opposite pressure pulse at $(x, r) = (25, -1)$. Color contours of the resulting pressure perturbation are shown to visualize the acoustic response. In the downstream direction, the response is contained within a Mach cone owing to the supersonic propagation of the disturbance by the jet. In the upstream and lateral directions, the response is bounded by a circle centered at $(x, r) = (25, 1)$ with radius $\bar{c}_0 t$ where $\bar{c}_0$ is the speed of sound in the exterior fluid.

Within this region, the developing wavepacket is composed of two parts: a growing portion near the leading edge of the Mach cone and a trailing neutral (or slightly damped) portion. The evolution of the wavepacket is visualized in Fig. 3(b), which displays the amplitude integrated over r plotted against group velocity at three different times. Clearly, the unstable portion of the wavepacket is restricted to downstream propagating group velocities, indicating convective instability. The maximum growth is obtained for $v_g = 0.72$ in good agreement with that associated with the Kelvin–Helmholtz instability wave reported by Malik & Chang (2000). At this group velocity, this wave still propagates supersonically with respect to the exterior fluid, and creates Mach waves in much the same way as does a supersonically propagating wavy wall (Tam 1995). The angle of the Mach wave radiation, indicated by the dashed line second-from-the-right, was found to be $\approx 54°$.

The trailing portion of the wavepacket, however, is observed to be close to neutral,

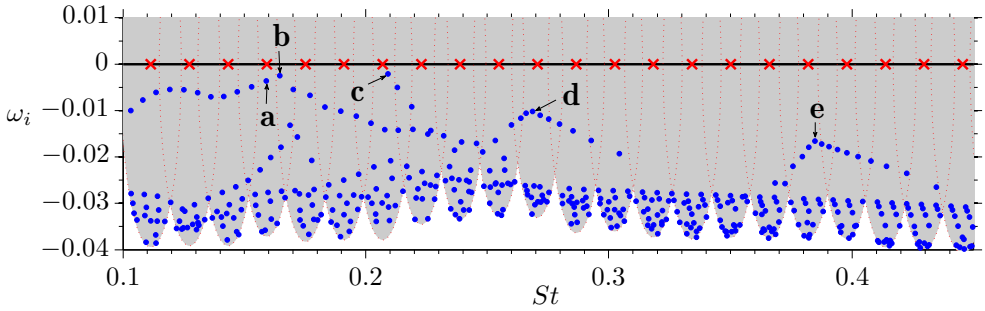

FIGURE 4. Eigenvalues (•) corresponding to global modes of the nonparallel supersonic jet. Twenty eigenvalues are converged for each shift (×). The unshaded portion of the plane represents locations where information is still missing.

and composed of waves traveling upstream at velocity $\bar{c}_0$, even inside the jet interior. This is possible because the disturbances within the jet core are attached to exterior acoustic waves. These waves correspond exactly to the subsonic family of instability waves predicted by Tam & Hu (1989). They exhibit a criss-crossed pattern within the core, with a predicted angle of $\psi = \sin^{-1}(\bar{c}_j/(u_j + \bar{c}_0)) \approx 14.5°$ from the horizontal, indicated by the crossed dashed lines. The third family of supersonic instability waves predicted by Tam & Hu (1989) is not observed in the present case because the Mach number is not sufficient to satisfy the necessary criterion $u_j > \bar{c}_j + \bar{c}_0$.

3.3. *Global modes of the nonparallel jet*

Fig. 4 shows a spectrum resulting from the shift-and-invert Arnoldi method applied to the nonparallel supersonic jet. The base flow was constructed by solving the compressible boundary layer equations with $Re = 3600$, $M = 2.5$, and $T_j/T_0 = 0.444$. To capture the least stable modes, the shifts (×) were selected along the real axis. For each shift, an Arnoldi method converged to the 20 nearest eigenvalues, using a Krylov subspace of size 54. The shaded circles (or ellipses) visualize the distance from each shift to the most remote eigenvalue in its group of 20. The circles appear as ellipses simply because of the aspect ratio of the axes. The shaded area therefore represents the area of the complex ω-plane in which the locations of the eigenvalues are known. The remaining unshaded area represents the portion of the plane in which information is still missing. If required, this missing information may be recovered either by increasing the number of converged eigenvalues sought at each shift, or by placing additional (generally complex) shifts at or beyond the frontier of the shaded region. The latter process can be repeated in a massively parallel manner until the entire ω-plane is covered. Note also that in the region near to the real axis, the circles tend to overlap so that eigenvalues obtained at one shift may be redundant to eigenvalues obtained at neighboring shifts. In practice, the mode shapes corresponding to these redundant eigenvalues agree well, providing an additional check on the convergence of the Arnoldi method.

In Fig. 4, the growth rate ω_i of each eigenvalue is plotted versus the Strouhal number, defined as $St = 2Rf/u_j = \omega_r/\pi$. Because all of the eigenvalues lie below the real axis, all of the modes are damped and therefore the flow is globally stable. The least damped portion of the spectrum, however, appears between $St \approx 0.1$ and $St \approx 0.2$. Figs. 5(a) and 5(b) show global modes corresponding to two neighboring eigenvalues representative

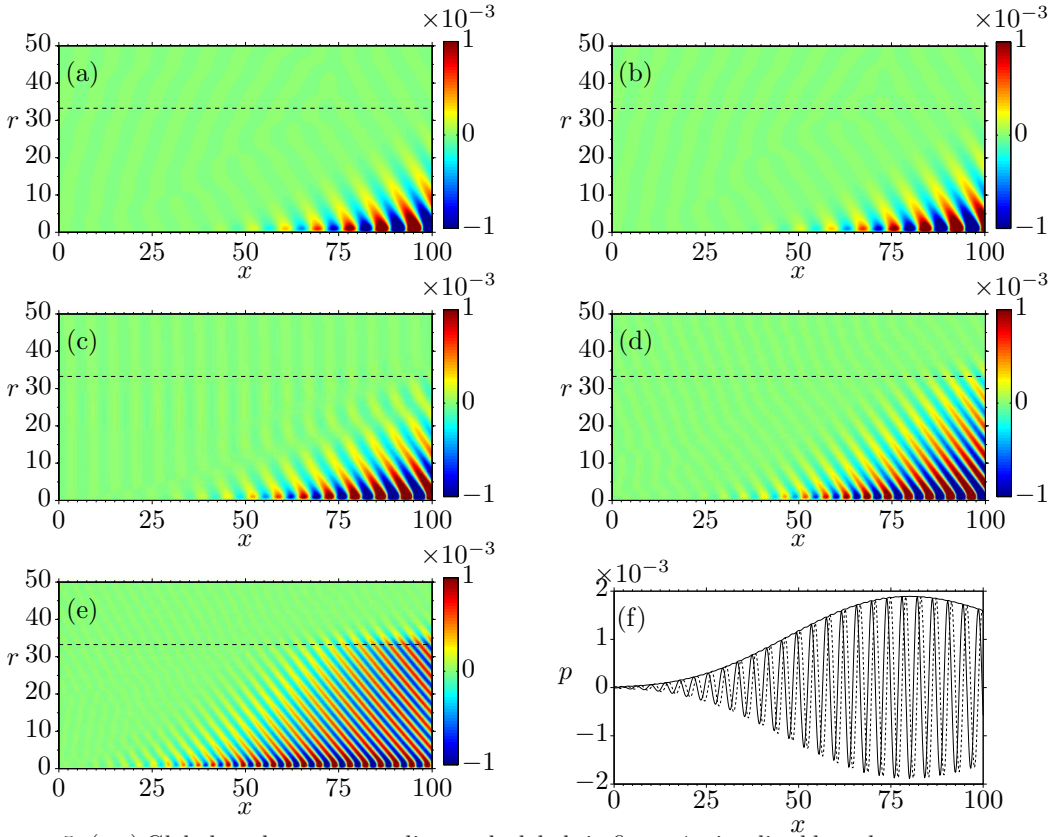

FIGURE 5. (a-e) Global modes corresponding to the labels in figure 4, visualized by color contours of the real part of pressure. (f) Real part ——— , imaginary part - - - - , and magnitude ——— of pressure along the line $r = 1$ for mode (e).

of this range. The dashed horizontal line at $r = 33.5$ in Figs. 5(a-e) represents the point at which r first becomes complex in the complex path implementation of the lateral boundary condition. Only the portion of the domain below this dashed line should be regarded as physical. In this region, global modes (a) and (b), aside from a phase difference, have almost identical shape. The similarity of neighboring global modes implies that the basis of global modes is highly non-normal. As we will see, this high degree of non-normality creates the potential for substantial transient growth. From a control systems perspective, the fact that the global modes obtain maximum amplitude near the outlet implies that the system response will be most observable in this downstream region. This is a direct consequence of the convection inherent to the base flow, where perturbations introduced upstream grow as they convect downstream, obtaining maximum amplitude just before they are convected out of the domain. For this reason, the system is said to exhibit "convective non-normality" (Chomaz 2005).

Three other groups of slightly damped eigenvalues are visible in the spectrum of Fig. 4. Representative global modes are shown in Figs. 5(c-e). As the frequency increases, the length scales tend to decrease. While global modes (c) and (d) have maximum amplitude at the outlet, mode (e) reaches maximum amplitude before the outlet, near $x = 80$. Fig. 5(f) shows the real and imaginary parts of this mode along the horizontal line $r = 1$. The Gaussian envelope of this mode is reminiscent of stability modes of a cold

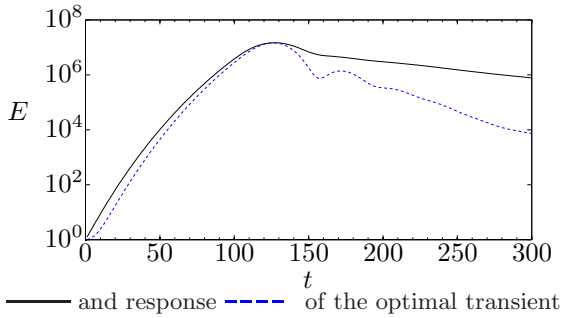

FIGURE 6. Envelope ——— and response - - - - of the optimal transient energy growth in the basis of the extracted global modes.

thin supersonic jet found by the PSE technique in Cheung *et al.* (2007), despite having slightly different flow parameters. For purely convectively unstable flows such as the cold supersonic jet, the PSE method is expected to perform well as it efficiently captures unstable downstream propagating waves. Therefore, the global and PSE modes should have similar shapes in this case. Note, however, that PSE modes discussed in Cheung *et al.* (2007) and Sandham & Salgado (2008) have real frequency and are temporally neutral. Thus, they require sinusoidal forcing to be sustained.

3.4. *Optimal superposition of global modes*

Even though all of the global modes of the cold supersonic jet are temporally damped, a large transient response is still possible through the superposition of these non-normal modes. In this section, we use a singular value decomposition to find the particular superposition that provides the largest transient growth. Because the converged global modes form a subset of the entire spectrum, this optimal superposition provides an approximation (more precisely, a lower bound) to the maximum attainable transient growth by system. Moreover, because the superposition is optimal, it is also the best possible approximation to the maximum transient response in this basis.

In order to fix our idea of growth of a perturbation, we must first choose an appropriate measure quantifying is amplitude. For incompressible flows, the kinetic energy of the perturbation is a natural choice. In the case of compressible flows, fluctuations in the pressure and entropy must also be taken into account. According to Chu (1965), the following definition of disturbance energy is positive definite and monotone non-increasing in time for perturbations about a compressible fluid at rest. This norm was independently derived by Hanifi *et al.* (1996) by eliminating the conservative compression work transfer terms in the evolution equation for the disturbance energy E.

$$E = \int\int \left[\frac{\bar{\rho} u_i u_i^*}{2} + \frac{M^2 |p|^2}{2} + \frac{\gamma(\gamma-1) M^2 |s|^2}{2} \right] r dr dx, \tag{3.2}$$

where * signifies the complex conjugate. This definition of disturbance energy norm induces the following inner product for two system states $\boldsymbol{q}_1$ and $\boldsymbol{q}_2$:

$$(\boldsymbol{q}_1, \boldsymbol{q}_2)_E = \boldsymbol{q}_2^H \boldsymbol{W} \boldsymbol{q}_1, \tag{3.3}$$

where $\boldsymbol{W} = 1/2 \operatorname{diag}\left(M^2,\ \bar{\rho},\ \bar{\rho},\ \bar{\rho},\ \gamma(\gamma-1)M^2\right)\ r \Delta r \Delta x$. Following Schmid & Henningson (2001), we can relate this energy norm to a standard Euclidean norm by expanding the system states in the basis of global modes $\boldsymbol{Q}$ so that $\boldsymbol{q}_1 = \boldsymbol{Q}\boldsymbol{\kappa}_1$ and $\boldsymbol{q}_2 = \boldsymbol{Q}\boldsymbol{\kappa}_2$. In

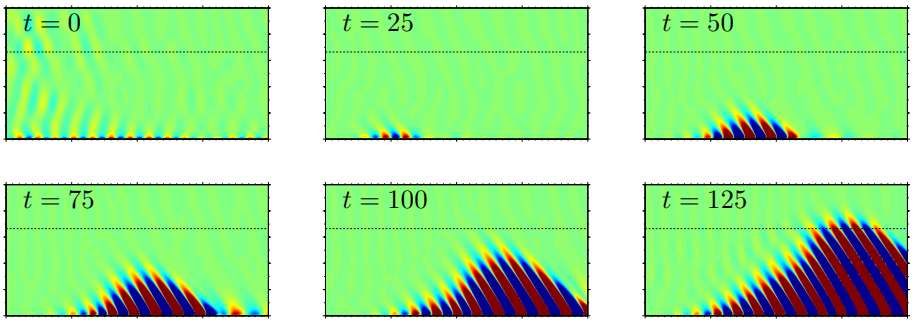

FIGURE 7. A time sequence of the optimal transient response in the basis of the extracted global modes. The color contour levels, representing pressure, are the same in each frame except for $t = 0$, where they are magnified by a factor of 5.

this case,

$$(\boldsymbol{q}_1, \boldsymbol{q}_2)_E = (\boldsymbol{Q}\boldsymbol{\kappa}_2)^H \boldsymbol{W} (\boldsymbol{Q}\boldsymbol{\kappa}_1) = \boldsymbol{\kappa_2}^H \left(\boldsymbol{Q}^H \boldsymbol{W} \boldsymbol{Q}\right) \boldsymbol{\kappa}_1 = \boldsymbol{\kappa_2}^H \boldsymbol{F}^H \boldsymbol{F} \boldsymbol{\kappa}_1 = (\boldsymbol{F}\boldsymbol{\kappa}_1, \boldsymbol{F}\boldsymbol{\kappa}_2)_2 , \tag{3.4}$$

where $\boldsymbol{F}$ is the square root of the Hermitian and positive definite matrix $\boldsymbol{M} = \boldsymbol{Q}^H \boldsymbol{W} \boldsymbol{Q}$.

Using this energy norm, we follow Schmid & Henningson (2001) and define $G(t)$ to be the maximum possible energy amplification at time t from any initial condition $\boldsymbol{q}_0$. In the subspace spanned by the global modes, this reduces to:

$$\begin{aligned} G(t) = \max \frac{||\boldsymbol{q}(t)||_E^2}{||\boldsymbol{q}_0||_E^2} &= \frac{||\boldsymbol{F}\boldsymbol{\kappa}(t)||_2^2}{||\boldsymbol{F}\boldsymbol{\kappa}_0||_2^2} = \frac{||\boldsymbol{F} e^{-it\boldsymbol{\Lambda}} \boldsymbol{\kappa}_0||_2^2}{||\boldsymbol{F}\boldsymbol{\kappa}_0||_2^2} \\ &= \frac{||\boldsymbol{F} e^{-it\boldsymbol{\Lambda}} \boldsymbol{F}^{-1} \boldsymbol{F}\boldsymbol{\kappa}_0||_2^2}{||\boldsymbol{F}\boldsymbol{\kappa}_0||_2^2} = ||\boldsymbol{F} e^{-it\boldsymbol{\Lambda}} \boldsymbol{F}^{-1}||_2^2, \end{aligned} \tag{3.5}$$

which is equal to the square of the largest singular value of the matrix $\boldsymbol{B} = \boldsymbol{F} e^{-it\boldsymbol{\Lambda}} \boldsymbol{F}^{-1}$. Here, we have used the fact that $\boldsymbol{\kappa}(t)$ evolves as $d\boldsymbol{\kappa}/dt = -it\boldsymbol{\Lambda}$ where

$$\boldsymbol{\Lambda} = \mathrm{diag}\left(\omega_1, \omega_2, \ldots, \omega_N\right), \tag{3.6}$$

with ω_i the eigenfrequency corresponding to each global mode.

The maximum transient growth $G(t)$ is plotted for the cold supersonic jet in Fig. 6. It is important to note that $G(t)$ is an envelope of all possible optimal responses, since the optimum initial condition $\boldsymbol{q}_0$ depends on the finite time interval t considered. $G(t)$ attains a maximum of 10^7 at $t = 125$. The particular optimal response for this time interval is shown by the blue dashed curve in Fig. 6, tangent to the envelope at $t = 125$. After $t = 125$, $G(t)$ decreases owing to the overall global stability of the system. This time corresponds to the time necessary for a disturbance moving with a convection velocity of $0.8u_j$ to propagate from the inlet to the outlet of the domain. This convection velocity is close to that of the maximally amplified portion of the wavepacket shown in Fig. 3(b).

Using the right singular vector corresponding to the largest singular value of $\boldsymbol{B}$, we can reconstruct the optimal initial condition needed to produce this response. A time series of the evolution of this response is shown in Fig. 7. At $t = 0$, the perturbation is initially distributed in x owing to the limited number of global modes included in

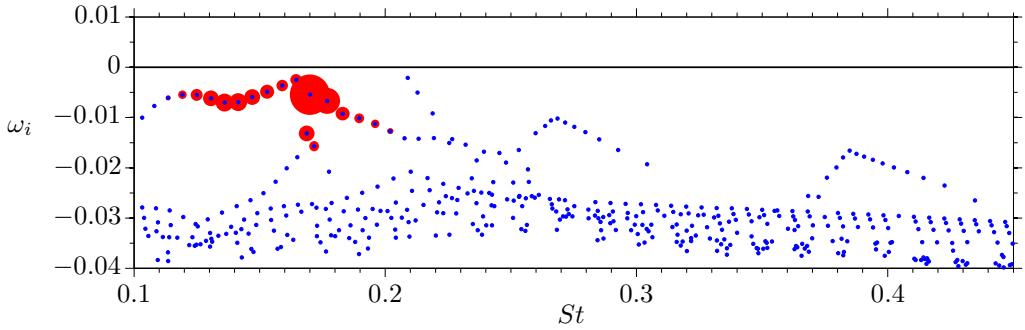

FIGURE 8. Contributions of individual global modes to the optimal transient response.

the basis considered. After the initial time, however, the response quickly resembles the development of a linear wavepacket owing to an impulse near the inlet. Clearly, through their non-normal superposition, the global modes have been successful in this case at capturing growth corresponding to a convective instability for locally parallel flow.

Finally, Fig. 8 visualizes the contributions of the individual global modes to the optimal response shown in Fig. 7. The radius of the red circle surrounding each eigenvalue is proportional to its contribution to the initial condition $\boldsymbol{q}_0$. Over most of the spectrum, the red circles are so small that they are hidden behind the blue dots indicating the locations of the eigenvalues. Evidently, the portion of the spectrum surrounding modes (a) and (b) shown in Fig. 4 plays the largest role in determining the transient response. Interestingly, the least damped mode of the system, mode (c), is almost completely irrelevant to the transient response.

4. Future work

We have demonstrated that non-normality is important for characterizing the dynamics of linearized disturbances in a non-parallel jet flow. Due to the supersonic convective nature of these disturbances in the cold $M = 2.5$ jet studied here, there is also a direct connection to the sound production in this supersonic jet. Although the cold supersonic jet is globally stable, a transient energy amplification of more than seven orders of magnitude was observed. In an experimental setting, background fluctuations would need to be kept below a factor of 10^{-7} of mean flow values to remove the possibility of observing this transient response. Because thermal fluctuations are usually well above this level, one might argue that this transient response will always be accessible in laboratory experiments. Note, however, that because this transient response is optimal, it represents the worst case scenario and the particular initial conditions that produce this growth may have a low probability of occurrence. If this probability is not vanishingly small, however, then sound production by this supersonic jet might be interpreted as a series of transient responses instigated by persistent low-level stochastic forcing.

It is important to point out that this result is not in conflict with the nonlinear mode interaction view of sound production. Rather, the optimal transient response might be used as a criterion selecting the set of linear waves that will amplify most efficiently to levels necessary for nonlinear interaction. A missing link in this analysis could provide a

means to evaluate the radiative efficiency of the nonlinear interactions involving this set of waves once they have reached sufficient amplitude. This might be accomplished by introducing the optimal perturbation as an initial condition to a fully nonlinear simulation and observing its acoustic response.

Finally, although the global mode analysis was able to capture the physics of a cold supersonic jet, it would be interesting to apply this method to cases where PSE breaks down. In particular, a comparison of the predictive performance of PSE versus global mode decomposition for a heated subsonic or transonic jet would be an excellent test.

Acknowledgments

The authors gratefully acknowledge support from NASA grant #NNX07AC94A, and thank O. Marxen of CTR for his careful reading of a preliminary version of this manuscript and for several insightful comments which have helped improve it significantly.

REFERENCES

Brown, G. L. & Roshko, A. 1974 On density effects and large structure in turbulent mixing layers. *Journal of Fluid Mechanics* **64**, 775.

Cheung, L. C., Bodony, D. J. & Lele, S. K. 2007 Noise radiation predictions from jet instability waves using a hybrid nonlinear pse-acoustic analogy approach. In *Proceedings of the 13th AIAA/CEAS Aeroacoustics Conference (28th AIAA Aeroacoustics Conference)*.

Cheung, L. C. & Lele, S. K. 2009 The dynamics of nonlinear instability waves in laminar heated and unheated compressible mixing layers. *Physics of Fluids* **21**, 094103.

Chomaz, J.-M. 2005 Global instabilities in spatially developing flows: Non-normality and nonlinearity. *Annual Review of Fluid Mechanics* **37**, 357–392.

Chu, B.-T. 1965 On the energy transfer to small disturbances in fluid flow (part i). *Acta Mechanica* **1**, 215–234.

Crighton, D. 1978 Orderly structure as a source of jet exhaust noise: Survey lecture. In *Structure and mechanisms of turbulence II*, *Lecture Notes in Physics*, vol. 76, p. 154170. Berlin/Heidelberg: Springer.

Ehrenstein, U. & Gallaire, F. 2005 On two-dimensional temporal modes in spatially evolving open flows: the flat-plate boundary layer. *Journal of Fluid Mechanics* **536**, 209–218.

Hanifi, A., Schmid, P. J. & Henningson, D. S. 1996 Transient growth in compressible boundary layer flow. *Physics of Fluids* **8**, 826.

Lehoucq, R. B., Sorensen, D. C. & Yang, C. 1998 *ARPACK Users' Guide: Solution of Large-Scale Eigenvalue Problems with Implicitly Restarted Arnoldi Methods*. SIAM.

Li, X. S. & Demmel, J. W. 2003 SuperLU_DIST: A scalable distributed-memory sparse direct solver for unsymmetric linear systems. *ACM Trans. Mathematical Software* **29** (2), 110–140.

Lu, G. & Lele, S. K. 1996 A numerical investigation of skewed mixing layers. *Tech. Rep.* TF-67. Dept. of Mech. Eng., Stanford University.

Malik, M. & Chang, C.-L. 2000 Nonparallel and nonlinear stability of supersonic jet flow. *Computers & Fluids* **29**, 327–365.

Michalke, A. 1984 Survey on jet instability theory. *Progress in Aerospace Sciences* **21**, 159–199.

Morrison, G. L. & McLaughlin, D. K. 1980 Instability process in low reynolds number supersonic jets. *AIAA Journal* **18**, 793–800.

Riedinger, X., Le Dizès, S. & Meunier, P. 2010 Viscous stability properties of a Lamb–Oseen vortex in a stratified fluid. *Journal of Fluid Mechanics,* In press.

Sandham, N. D., Morfey, C. L. & Hu, Z. W. 2006 Nonlinear mechanisms of sound generation in a perturbed parallel jet flow. *Journal of Fluid Mechanics* **565**, 1.

Sandham, N. D. & Salgado, A. M. 2008 Nonlinear interaction model of subsonic jet noise. *Philosophical transactions. Series A, Mathematical, physical, and engineering sciences* **366**, 2745–60.

Schmid, P. J. & Henningson, D. S. 2001 *Stability and Transition in Shear Flows*. New York: Springer-Verlag.

Suponitsky, V. & Sandham, N. D. 2009 Nonlinear mechanisms of sound radiation in a subsonic jet. In *Proceedings of the 15th AIAA/CEAS Aeroacoustics Conference (30th AIAA Aeroacoustics Conference)*, pp. 1–21. Miami.

Tam, C. K. W. 1995 Supersonic jet noise. *Annual Review of Fluid Mechanics* **27**, 17–43.

Tam, C. K. W. & Burton, D. E. 1984 Sound generated by instability waves of supersonic flows. part 2. axisymmetric jets. *Journal of Fluid Mechanics* **138**, 273.

Tam, C. K. W. & Hu, F. Q. 1989 On the three families of instability waves of high-speed jets. *Journal of Fluid Mechanics* **201**, 447–483.

Wu, X. & Huerre, P. 2009 Low-frequency sound radiated by a nonlinearly modulated wavepacket of helical modes on a subsonic circular jet. *Journal of Fluid Mechanics* **637**, 173.